Optics Letters

Photonic nanojet of cylindrical metalens assembled by hexagonally arranged nanofibers for breaking the diffraction limit

LIYANG YUE,[1,*] BING YAN,[1] AND ZENGBO WANG[1,2]

[1]School of Electronic Engineering, Bangor University, Dean Street, Bangor, Gwynedd LL57 1UT, UK
[2]e-mail: z.wang@bangor.ac.uk
*Corresponding author: l.yue@bangor.ac.uk

Received 8 January 2016; revised 16 February 2016; accepted 16 February 2016; posted 17 February 2016 (Doc. ID 256945); published 16 March 2016

We designed a novel cylindrical metalens assembled by hexagonally arranged close-contact nanofibers. A near-field focusing nanojet with a full-width at half-maximum (FWHM) waist, 26.7% smaller than the Abbe diffraction limit for 532 nm wavelength light, is observed at the bottom of a 1600 nm diameter cylindrical metalens assembled by 160 nm diameter nanofibers irradiated by a plane wave from the top. Using differently sized nanofibers as building blocks to assemble the metalens, the waist size of the produced photonic nanojet in the near-field zone and the lateral resolution of the focus can be flexibly adjusted, simultaneously breaking the diffraction limit.

OCIS codes: (160.3918) Metamaterials; (290.0290) Scattering; (050.1940) Diffraction; (230.0230) Optical devices.

http://dx.doi.org/10.1364/OL.41.001336

The Abbe diffraction limit, $\lambda/2n_1$, defines the size of the smallest feature that can be observed by an optical imaging system, where λ is the wavelength of the incident light, and n_1 is the refractive index of the light-traveling medium. A photonic nanojet is a narrow and high-intensity electromagnetic beam that propagates into the background medium after focusing a plane wave with a dielectric microcylinder or microsphere, whose diameter is greater than the wavelength of the plane wave [1]. Lu *et al.* first demonstrated this enhanced optical near-field phenomenon using a micro silica sphere in 2000 [2]; then, in 2004, Chen *et al.* found that a transparent dielectric microcylinder with a wavelength-scale radius can generate a similar effect and produced a FWHM waist that was slightly smaller than $\lambda/2$ [3]. Since then, the properties of these scattering distributions have been explored both analytically and numerically by previous researchers [4–6], and the relationship between the microsphere/cylinder, the photonic nanojet, and the refractive index of medium has been explored. Li *et al.* reported that both the maximum intensity and the FWHM waist of the nanojet increase with the growth of the microsphere diameter [7]. Guo *et al.* indicated that the ideal refractive index contrast between the microsphere material and the surrounding medium to obtain a higher numerical aperture (NA) for the microsphere is about 1.5–1.75 [8]. Also, in the imaging application field, Wang *et al.* invented a 50 nm resolution nanoscope that uses a photonic nanojet of optically transparent microspheres to overcome the white light DL, and this achievement is used in the application of *in vivo* observations for life science research [9].

On the other hand, negative refraction and metal-based metalenses (e.g., the Pendry superlens) [10] and hyperlens [11] have been developed and have gained huge interest in the past decade. These developments are benefiting from the huge progress achieved in plasmonics and metamaterials research, which provides possibilities for artificially manipulating material properties not found in nature, e.g., negative refractive index and anisotropic materials [12]. It is well known that subwavelength information carried by an evanescent wave cannot be collected by a conventional optical lens and contribute to imaging because evanescent waves are nonpropagating in a normal material environment, which is the meaning of a DL in the frequency domain [11]. In order to acquire this ability, a metalens is capable of converting high wave vector waves to low wave vector waves and making their information collectable, which is called magnification mechanism [12]. Some of the early metalenses possessed superresolution; however, they were not able to focus plane waves because of the lack of a phase compensation mechanism. Contrarily, a conventional optical lens can focus a plane wave via a curved surface due to fundamental optics Fourier transforms [10]. Subsequently, various metalens designs emerged and simultaneously had both functions through matching the phase condition by using plasmonic waveguide couplers (PWC) [13–16] and gradient-index (GRIN) metamaterials with refractive-index variations [17,18].

In this Letter, we seek the combination of the metamaterial concept with a photonic nanojet. The idea is to use nanofibers as building blocks to create a microsized artificial metalens. By varying the compositional nanofiber diameter, we shall be able to tune the focusing property of the metalens according to our needs. Our work is new and has never been reported before in the literature. Using a full-wave simulation approach (CST

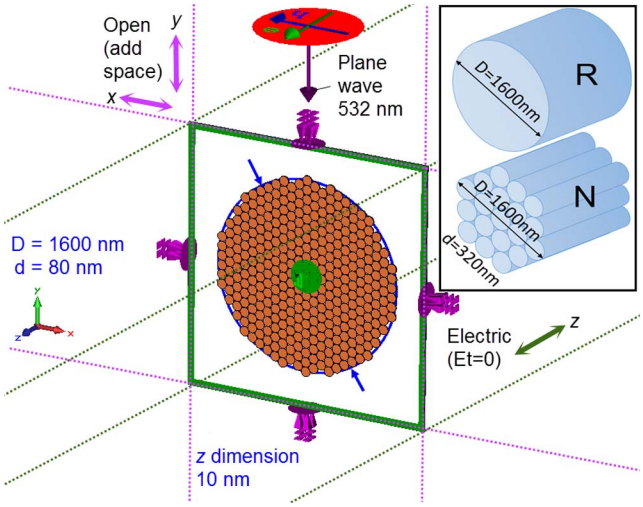

Fig. 1. CST model ($D = 1600$ nm and $d = 80$ nm) and the applied boundary conditions, with the inset containing diagrams of (R) the reference microcylinder and (N) the nanofiber metalens with $d = 320$ nm.

studio), we investigated the field propagation of a plane wave ($\lambda = 532$ nm) passing through a $D = 1600$ nm diameter cylinder metalens assembled by hexagonally arranged nanofibers ($n_1 = 1.5$) in the air (refractive index of background medium, $n_2 = 1$) and found that superresolution will be generated with FWHM waists of triggered photonic nanojets much smaller than the Abbe diffraction limit. To understand the mechanism, the nanofibers' diameters were varied ($d = 40$, 80, 160, 320, and 640 nm) in the simulation. The obtained field distributions were also compared to a reference, which was a homogeneous material microcylinder with the same 1600 nm diameter and refractive index, $n_1 = 1.5$. Meanwhile, we also plotted the power flow streamlines for the homogenous reference and the composite (for nanofibers with 640 nm diameters) metalens, which reveal the complex nature of the light flows in micro/nano scales.

Geometrically, this novel metalens is structured such that multiple hexagonally arranged close-contact nanofibers fully fill a cylindrical space with a certain diameter of 1600 nm; accordingly, the number of nanofibers is inversely proportional to the thickness of the nanofibers due to the fixed cross-sectional area of the metalens. The diagram of the $d = 320$ nm metalens is shown in the inset of Fig. 1. A 532 nm wavelength plane wave is incident at the top of the metalens with a transverse magnetic (TM) mode, where the incident magnetic field vector is perpendicular to the axis of the cylindrical metalens cross section. While the cross section is on the x–y plane, the axis of regard is placed along the z axis, as shown in Fig. 1. To simulate a nanofiber's large ratio of length to diameter, the length of the metalens along the z axis is defined as infinitely long via the proper boundary condition "electric ($E_t = 0$)," which means that at the z-axis direction, the metalens will operate like a perfect electrical conductor, and a model with a small z-axis dimension (10 nm) can guarantee the accuracy of the calculation and reduce the number of meshes. At the x- and y-axis directions, the boundary conditions are both "open (add space)" to leave enough space to present electronic and power flow distributions of light in the background medium–air, as shown in Fig. 1. The refractive index of the nanofiber, n_1, is set to 1.5, and background medium is air, whose refractive index, n_2, is 1. Also, the same modeling conditions are applied to the reference model, which is a 1600 nm diameter microcylinder of homogeneous material without the nanofiber assembly; the diagrams for it are in the inset of Fig. 1.

Figure 2(a) presents the classical two-dimensional (2D) electric field enhancement, E^2, distribution (x–y plane) of a microcylinder made of a homogeneous material ($n_1 = 1.5$), which is the reference with the same modeling conditions as the novel metalens assembled by nanofibers. It shows that a plane wave propagates from the top, and the typical microcylinder near-field focusing effect is observed. Consequently, there is an intensity peak of the electric field, known as the photonic nanojet, at the bottom of the cross section of the microcylinder. Its E^2 enhancement is about 7.84, compared to standard plane wave intensity of 1, and the FWHM waist is 198 nm, larger than the DL of the 532 nm wavelength plane wave (177.3 nm). The same figures representing novel cylinder metalenses assembled with nanofibers of five different diameters ($d = 40$, 80, 160, 320, and 640 nm) are shown in Figs. 2(b)–2(f). With a decrease in nanofiber diameter, the frequency of the alternating change in refractive index is larger due to the smaller space left for background medium–air in the metalens. In fact, the electric field distributions of the metalenses, as shown in Figs. 2(b)–2(f), are similar to that of the reference model in Fig. 2(a). The focusing effect still plays the most important role in the propagation of the plane wave in the metalens, and the photonic nanojet is located at the interior of the nanofiber at the lowest position of the cross section. Thus, compared to reference model, photonic nanojets created by different sized nanofiber assembled metalenses have much stronger E^2 electric field enhancement and smaller FWHM waists. Their E^2 profiles at the most enhanced position are plotted along the x axis in Fig. 2(g), and all results are also summarized in Fig. 2(h). These indicate that a batch of nanofibers is able to focus a spot far smaller than that of the reference, even at the Abbe diffraction limit. The Abbe diffraction limit of 532 nm wavelength light (DL = 177.3 nm) and the FWHMs of nanojets generated by the reference (198 nm) and the $d = 160$ nm nanofiber metalens (130 nm) are marked for comparison in Fig. 2(g). In Fig. 2(h), a dashed line to show DL appears at the 177.3 nm position on the x axis. All scatters representing the metalenses are on the left of the dashed line, while only the scatter for the reference is on its right. The smallest FWHM waist (130 nm) achieved by the $d = 160$ nm model is 26.7% smaller than the DL. Meanwhile, the highest E^2 enhancement of the electric field is delivered by the same model, reaching 17.242, larger than that for the other sizes of nanofibers, and almost 2.2 times that of the reference model in this case. When used in superresolution imaging applications, these metalenses will be used in combination with a conventional objective lens. When the metalens focus is located inside it, as in the cases of Figs. 2(b)–2(f), a magnified real image will be formed. Otherwise, a magnified virtual image will be formed when the focus is located outside of the lens body, like the reference case of Fig. 2(a) [9]. It should be noted that the cylindrical metalens generates a 1D superresolution image along the fiber. However, a complete large-area 2D superresolution image can be obtained by rotating the cylindrical fiber lens in a circular manner.

It is obvious that the improved superresolution in the proposed metalens originates from the introduced material inhomogeneity. The metalens is essentially a dense multiple scattering media with varying effective refractive index along the propagation direction. In such media, the optical fields evolve through both homogenous and evanescent waves. New regimes of light transport emerge because of the near-field coupling between individual scattering centers at mesoscopic scales [19]. The excited evanescent waves in the artificial media carry higher spatial frequency components and are essential to gaining higher spatial resolution beyond the DL. In homogenous media (reference case), however, no evanescent wave components will be excited inside the lens body, and its resolution is limited by diffraction. DL circle in frequency field is shown in Fig. 3(a), where k_x and k_y are wave vectors along the x and y axes, n_{eff} is effective refractive index along propagation direction, and k_0 is the incident beam wave vector. For metalens k_x factor identifies lateral resolution and it is possible to be larger than the circle radius and plays the most important role to obtain FWHM waist smaller than DL. In addition, the superresolution and the relationship between nanostructures and light frequency in the proposed metalens may have a physical connection with the photonic crystal, which is a material using a regular arrangement of structures, e.g., nanospheres, to attain a spatial periodicity in their dielectric constant in order to bend or inhibit the propagation of a certain light frequency [20].

At micro and nano scales, light interacts with objects differently than what is expected from geometrical optics in a ray trace picture. Full-wave simulations have revealed the very complex nature of light power flow at such scales [21,22]. Figures 3(b) and 3(c) show the streamlines of power flow for the reference microcylinder and the metalens assembled from nanofibers with

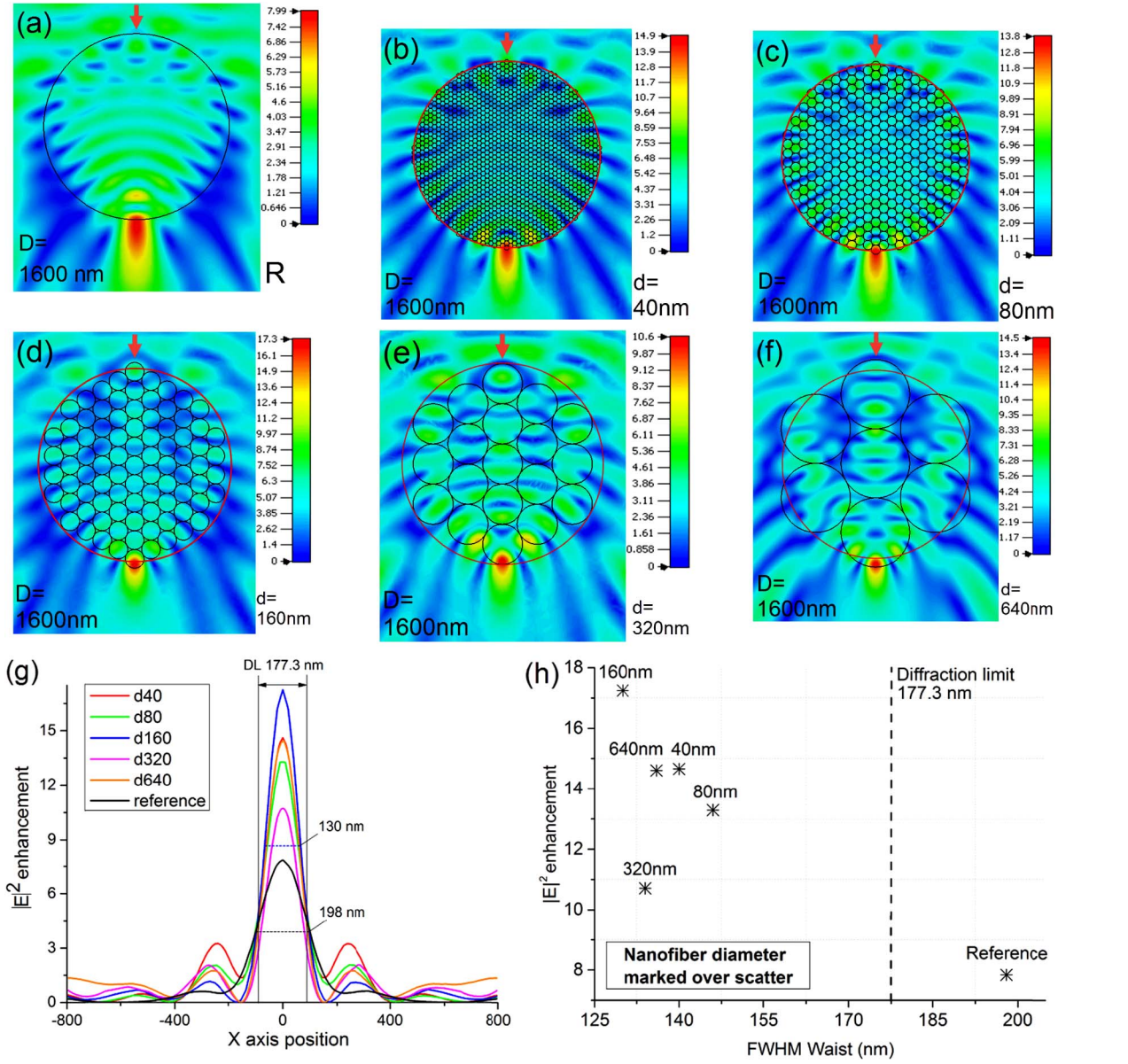

Fig. 2. (a)–(f) 2D electric field distributions for the reference (homogeneous) and metalenses assembled with nanofibers with $d = 40$, 80, 160, 320, and 640 nm, respectively. (g) E^2 profiles of the most enhanced positions along the x axis for the nanofiber metalenses and the reference. (h) Electric field enhancement and FWHM waists of metalenses derived from different diameter nanofibers.

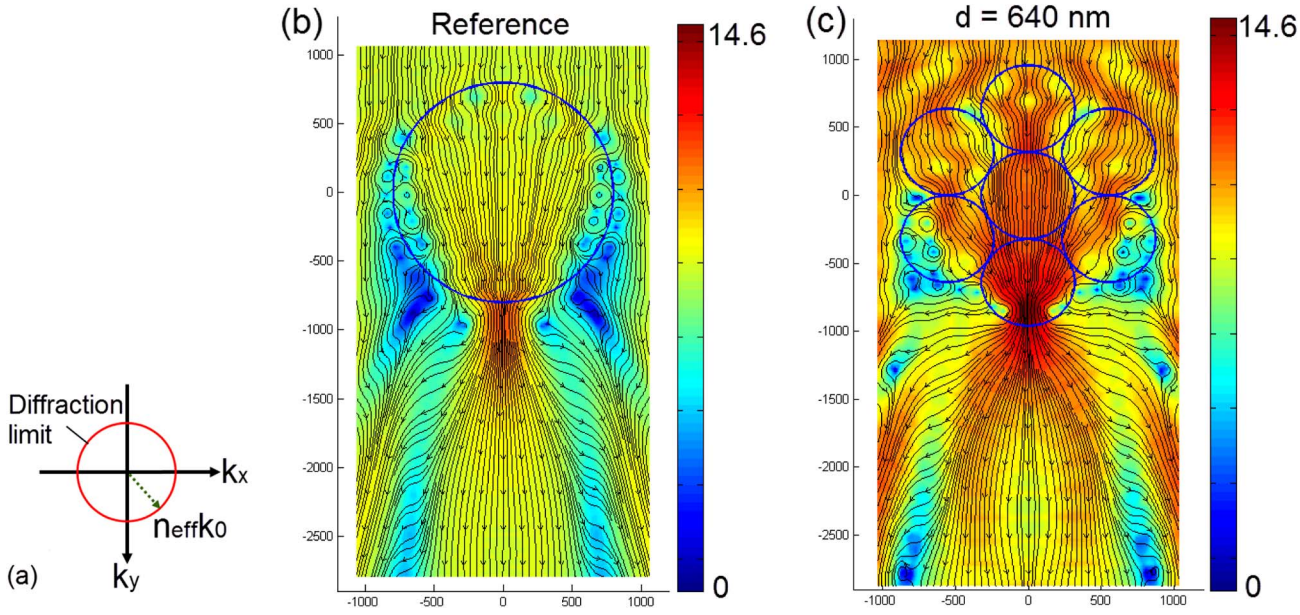

Fig. 3. (a) Diffraction limit curve in the frequency field. (b) Streamlines of power flow for reference microcylinder model. (c) Streamlines of power flow for a metalens assembled with 640 nm diameter nanofibers.

640 nm diameters. From Fig. 3(b), it can be noted that there are several singular points located around the edge of the reference microcylinder. The phase trajectories in the vicinities of the singular points form the clockwise vortexes that are in the relatively low electric intensity areas. It is known that phase trajectories of the system contain 1.5 degrees of freedom in the vicinity of the singular points, and the related clockwise vortex shape represents a stable focus in the phase space [23]. Also, power flow couples to the other planes through these singular points [22], which are caused by relatively low field intensity in these areas. Meanwhile, the nanofiber-assembled metalens has few singular points, as shown in Fig. 3(c), which indicates that more energy could be used for focusing on the same phase. An individual nanofiber still functions like a single nanolens, and an alternating refractive index change due to a novel hexagonal arrangement is capable of driving and guiding the power flow to the bottom nanofiber and maintaining a strong focus with outstanding electric intensity for the photnic nanojet. In Fig. 3(c), there are three obviously high-intensity streams (dark red) entering the metalens from the top three nanofibers, and their intensities increase after passing through them. Finally, these three high-intensity streams converge at the bottom of the lowest positioned nanofiber, which results in an area in the metalens whose electric field intensity is 14.608 times enhanced.

In conclusion, after numerical simulation, a cylindrical metalens assembled by hexagonally arranged transparent nanofibers ($n_1 = 1.5$) can successfully achieve lateral resolution beyond the Abbe diffraction limit ($\lambda/2n$) under the irradiation of 532 nm wavelength light in air ($n_2 = 1$) for imaging applications, and the smallest FWHM waist of photonic nanojet is only 130 nm, which is 26.7% smaller than the DL. A hexagonal arrangement of the nanofiber material leads to an alternating change of refractive index between that of air and nanofiber material, which effectively develops homogenous and evanescent waves accompanied with near-field coupling of scattering centers, and moreover, compresses the waist size and focuses more power flow for the subsequent photonic nanojet.

Funding. Welsh Government, UK, Sêr Cymru National Research Network in Advanced Engineering and Materials (NRNF66, NRN113).

REFERENCES

1. A. Heifetz, S.-C. Kong, A. V. Sahakian, A. Taflove, and V. Backman, J. Comput. Theor. Nanosci. **6**, 1979 (2009).
2. Y. F. Lu, L. Zhang, W. D. Song, Y. W. Zheng, and B. S. Luk'yanchuk, J. Exp. Theor. Phys. Lett. **72**, 457 (2000).
3. Z. Chen, A. Taflove, and V. Backman, Opt. Express **12**, 1214 (2004).
4. D. McCloskey, J. Wang, and J. F. Donegan, Opt. Express **20**, 128 (2012).
5. A. V. Itagi and W. A. Challener, J. Opt. Soc. Am. A **22**, 2847 (2005).
6. S. Lecler, Y. Takakura, and P. Meyrueis, Opt. Lett. **30**, 2641 (2005).
7. X. Li, Z. Chen, A. Taflove, and V. Backman, Opt. Express **13**, 526 (2005).
8. H. Guo, Y. Han, X. Weng, Y. Zhao, G. Sui, Y. Wang, and S. Zhuang, Opt. Express **21**, 2434 (2013).
9. Z. Wang, W. Guo, L. Li, B. Luk'yanchuk, A. Khan, Z. Liu, Z. Chen, and M. Hong, Nat. Commun. **2**, 218 (2011).
10. J. B. Pendry, Phys. Rev. Lett. **85**, 3966 (2000).
11. Z. Liu, H. Lee, Y. Xiong, C. Sun, and X. Zhang, Science **315**, 1686 (2007).
12. D. Lu and Z. Liu, Nat. Commun. **3**, 1205 (2012).
13. B. Ma and Z. W. Liu, Appl. Phys. Lett. **96**, 183103 (2010).
14. B. Ma and Z. W. Liu, J. Nanophoton. **5**, 051604 (2011).
15. Z. Sun and H. K. Kim, Appl. Phys. Lett. **85**, 642 (2004).
16. L. Verslegers, P. B. Catrysse, Z. Yu, J. S. White, E. S. Barnard, M. L. Brongersma, and S. Fan, Nano Lett. **9**, 235 (2009).
17. B. Ma, M. A. Escobar, and Z. W. Liu, Phys. Rev. B **84**, 195142 (2011).
18. H. F. Ma, G. Z. Wang, W. X. Jiang, and T. J. Cui, Sci. Rep. **4**, 6337 (2014).
19. R. R. Naraghi, S. Sukhov, J. J. Saenv, and A. Dogariu, Phys. Rev. Lett. **115**, 203903 (2015).
20. L. Novotny and B. Heght, *Principles of Nano-Optics* (Cambridge University, 2006), p. 363.
21. L. Yue, B. Yan, M. Attridge, and Z. B. Wang, Sol. Energy **124**, 143 (2016).
22. Z. B. Wang, B. S. Luk'yanchuk, M. H. Hong, Y. Lin, and T. C. Chong, Phys. Rev. B. **70**, 035418 (2004).
23. N. V. Karlov, N. A. Kirchenko, and B. S. Luk'yanchuk, *Laser Thermochemistry: Fundamentals and Applications* (Cambridge International Science, 2000), pp. 54–59.